

## Urea-based amino sugar agent clears murine liver and preserves protein fluorescence and lipophilic dyes

Michelle Hough<sup>1</sup>, Michael Fenlon<sup>1</sup>, Alison Glazier<sup>1</sup>, Celia Short<sup>1</sup>, Gerardo Esteban Fernandez<sup>1</sup>, Jiabo Xu<sup>1</sup>, Elaa Mahdi<sup>1</sup>, Kinji Asahina<sup>2</sup> & Kasper S Wang<sup>\*,1</sup> 

<sup>1</sup>Developmental Biology, Regenerative Medicine & Stem Cell Program, The Saban Research Institute, Children's Hospital of Los Angeles, Los Angeles, CA 90027, USA;

<sup>2</sup>Southern California Research Center for ALPD & Cirrhosis, Department of Pathology, Keck School of Medicine, University of Southern California, Los Angeles, CA 90089, USA; \*Author for correspondence: kwang@chla.usc.edu

BioTechniques 70: 73–80 (February 2021) 10.2144/btn-2020-0063

First draft submitted: 30 April 2020; Accepted for publication: 29 October 2020; Published online: 20 January 2021

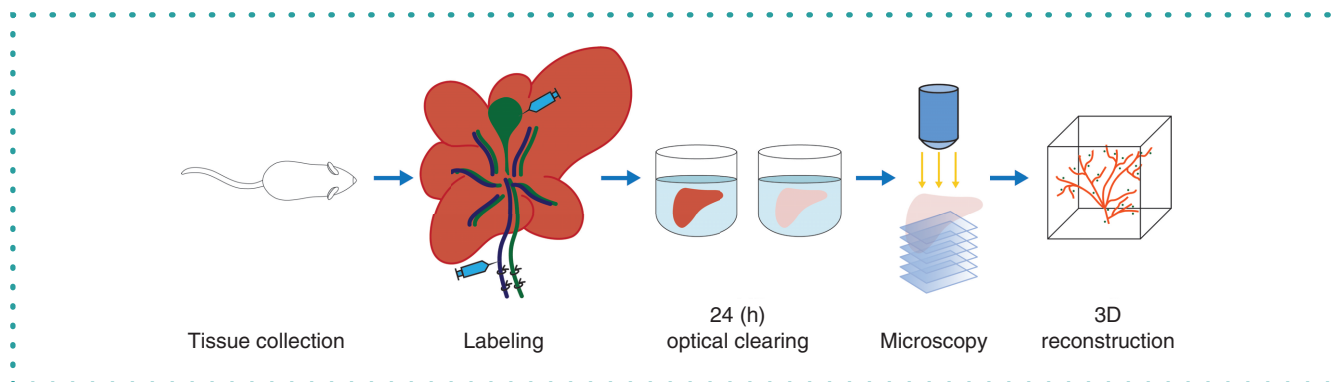
### ABSTRACT

Five established clearing protocols were compared with a modified and simplified method to determine an optimal clearing reagent for three-dimensionally visualizing fluorophores in the murine liver, a challenging organ to clear. We report successful clearing of whole liver lobes by modification of an established protocol (UbasM) using only Ub-1, a urea-based amino sugar reagent, in a simpler protocol that requires only a 24-h processing time. With Ub-1 alone, we observed sufficiently preserved liver tissue structure in three dimensions along with excellent preservation of fluorophore emissions from endogenous protein reporters and lipophilic tracer dyes. This streamlined technique can be used for 3D cell lineage tracing and fluoroprobe-based reporter gene expression to compare various experimental conditions.

### METHOD SUMMARY

This study presents a simplified protocol for optically clearing murine liver tissue in only 24 h using one simple urea-based amino sugar solution and a single incubation. This method preserves fluorescence of transgenically expressed proteins and lipophilic tracer dyes within the context of native spatial morphology.

### GRAPHICAL ABSTRACT



### KEYWORDS:

3D imaging • bile duct ligation • computational imaging • fluorescence microscopy • lipophilic tracers • liver clearing • optical clearing agents • prominin-1

Over the past several decades, optical clearing techniques have been developed to visualize large tissue volumes or small whole organisms in order to evaluate structural organization and patterning of functional consequence [1–7]. Optical clearing techniques coupled with 3D microscopy, such as confocal microscopy, light sheet fluorescence microscopy, optical projection tomography and ultramicroscopy [8,9], improve qualitative and quantitative evaluation of structural information that may be limited in single 2D tissue sections [8].

Protocols utilizing optical clearing agents (OCAs) reduce inherent variations in refractive index (RI) within tissues, while decreasing light scatter in order to render them transparent [10]. The various published OCAs offer different advantages and disadvantages in

terms of depth of clearance, preservation of fluorescent reporters, immunofluorescence compatibility, sample distortion, cost, toxicity, handling and speed [1,11–13]; some of these protocols take 1–2 weeks to complete. These techniques have been used to optically clear brain tissue, although other organs have also been studied [1,13–15].

Numerous challenges exist when attempting to optically clear the liver. Denser organs such as the liver typically require longer processing times to optically clear given their greater protein content [16] and pigmentation [17,18]. While OCAs ideally preserve fluorescent labeling [1], the emissions of commonly used fluorophores such as green fluorescent protein (GFP) are unfortunately quenched with some of more effective clearing protocols [11,14,19–21]. Fluorescent lipophilic dyes, such as Di-I, are taken up within intact membranes [19,22–27], making them incompatible with clearing protocols that rely heavily on delipidating detergents or organic solvents [14,28]. Nevertheless, a number of OCAs – such as BABB [29], SeeDB [30], ScaleS [12], UbasM [28], clear unobstructed brain/body imaging cocktails and computational analysis (CUBIC) [12,18], CLARITY-electrophoretic tissue clearing (CLARITY-ETC) [3] and active CLARITY technique-pressure related efficient and stable transfer of macromolecules into organs (ACT-PRESTO) [31] – have been used to optically clear the liver, albeit with some limitations.

Here, we report the use of Ub-1, the initial reagent in the multistep UbasM clearing protocol. The UbasM protocol requires nearly 2 weeks of processing time. Ub-1, however, adequately clears the murine liver with preservation of transgenically expressed fluorophores and infused lipophilic dyes in only 1 day. We compare the performance of Ub-1 with that of BABB and iDISCO, ScaleS, SeeDB and the complete UbasM protocol. We show that Ub-1 is an effective and time-efficient OCA for the murine liver that is useful for cell lineage tracing experiments.

## Materials & methods

### Mice

For the whole-mount 3D-imaged experiment with lipophilic dyes, we generated *Prom1<sup>CreERT2-nLacZ/+</sup>;Rosa26<sup>Lsl-GFP+</sup>* mice (obtained from R Gilbertson and Jackson Laboratory, #006148, respectively) in a C57BL/6 background [32]. At 6 weeks of age, mice were injected intraperitoneally with tamoxifen at a dose of 200 µg/g body weight. 1 week post-injection, the mice were euthanized by carbon dioxide asphyxiation. A midline incision was made from pubis to sternal notch, providing full exposure of the abdominal and thoracic cavity. A right ventriculotomy was performed and approximately 20 ml phosphate-buffered saline (PBS) was infused systemically via the left ventricle using a 25-gauge needle until effluent from the right ventricle was clear. The extrahepatic portal structures were then identified, and the common bile duct and portal vein individually ligated using 5.0 silk suture. Two hundred microliter of Vybrant<sup>®</sup> Di-D dye (Thermo Fisher Scientific; 1:1 dilution in PBS), with absorbance and fluorescence emissions of 644 and 665 nm respectively, was injected into the dome of the gallbladder, and 1 ml of Di-I (1:1 dilution in PBS) (absorbance and fluorescence emissions of 549 and 565 nm, respectively) into the portal vein. Livers were then collected and individual lobes separated for further processing.

For the whole-mount 3D-imaged injury experiments, we generated *C57BL/6 Prom1<sup>CreERT2-nLacZ/+</sup>;Rosa26<sup>Lsl-tdTomato</sup>;Collagen1a1 (Col1a1)<sup>GFP</sup>* mice (the latter two from Jackson Laboratory [#007914] and D Brenner, respectively) [33,34]. These triple transgenic mice underwent bile duct ligation (BDL) or sham laparotomy as previously described [33]. Fourteen days after BDL or the sham procedure, the mice were euthanized and the liver flushed as described above. Di-D was injected into the gallbladder with retrograde filling of the bile duct. For standard immunofluorescence, *Prom1<sup>CreERT2-nLacZ/+</sup>;Rosa26<sup>mTmG</sup>* mice (Jackson Laboratory, #007676) liver lobes were collected for processing 14 days after BDL or the sham operation. All animal experiments were conducted under a protocol approved by the Children's Hospital Los Angeles Institutional Animal Care and Use Committee.

### Clearing protocols

Liver lobes were fixed in 4% paraformaldehyde at 4°C overnight and dehydrated in 30% sucrose/PBS at 4°C for 24 h. Tissue was embedded in Tissue-Tek OCT<sup>®</sup> compound and frozen at -80°C until ready for clearing. Lobes were thawed in PBS. Our modified protocol for clearing was taken from the UbasM protocol described by Chen *et al.* [28]. The UbasM protocol for whole organ clearing consists of three steps: immersion in Ub-1 (25% meglumine, 25% urea, 20% 1,3-dimethyl-2-imidazolidinone, 0.2% Triton<sup>™</sup>-X100 and 29.8% water; RI: ~1.45) for 3–5 days at 37°C, followed by PBS for 12 h at 4°C, then immersion in Ub-2 at 37°C for 3–5 days. In our modified clearing protocol, we excluded the Ub-2 step, using only Ub-1 at 37°C on a gentle rocker for only 24 h. Cleared lobes were then directly imaged by confocal microscopy. Our step-by-step protocol can be viewed at [dx.doi.org/10.17504/protocols.io.bfs2jnge](https://dx.doi.org/10.17504/protocols.io.bfs2jnge). For comparison purposes, liver lobes were cleared using published protocols for agents BABB (RI: ~1.56) [35,36], iDISCO (RI: 1.56) [23,37], ScaleS (RI: 1.44) [23], SeeDB (RI: 1.50) [24] and UbasM (RI: ~1.47–1.48) [28].

### Confocal microscopy, transmission analysis & optical density

Liver lobes were imaged on a Zeiss LSM 710 confocal system mounted on an Axio Observer.Z1 microscope equipped with a C-Apochromat 10×/0.45 water-immersion lens (Carl Zeiss Microscopy, NY, USA). Z-stacks were acquired with 488, 561 and 633 nm laser light to excite GFP, Di-I and tdTomato, and Di-D, respectively. The confocal pinhole was set at 1 Airy unit and the z-interval at 5 µm. 3D volumes were rendered with Vision 4D software (arivis AG, Rostock, Germany). To collect images for optical density (OD) calculations, the microscope was adjusted for Köhler illumination and brightfield images were acquired with 405, 458, 488, 514, 561 and 633 nm laser light using the transmitted light detector. A z-stack of inherent tissue fluorescence was acquired with the 514-nm laser and a z-interval of

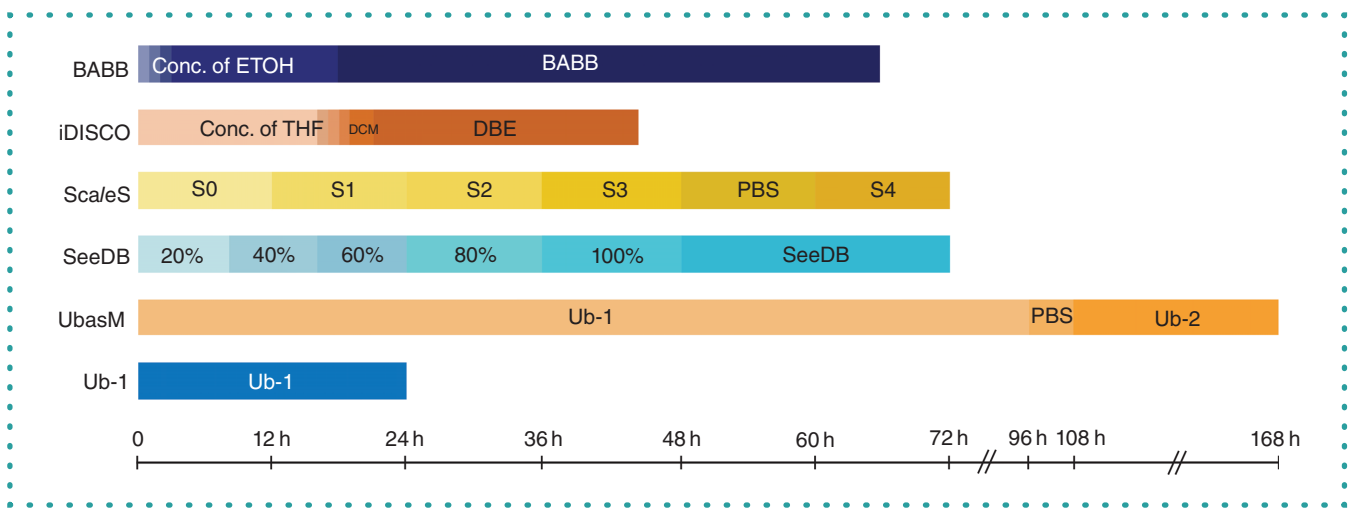


**Figure 1. Temporal comparison of optical clearing methods tested.** Whole liver lobes were cleared with BABB, iDISCO, Sca/eS, SeeDB, UbasM and Ub-1 reagents according to the timeline (shown in hours).

50  $\mu\text{m}$  to measure specimen thickness. Thickness and percentage transmittance were quantified with FIJI Image J (NIH, MD, USA) [38]. Z-stacks were resliced to generate orthogonal projections of each specimen and the thickest part in the field of view was measured. The observed thickness was adjusted to correct for RI mismatch by the ratio of the RI of the OCA to that of water. To measure transmittance, regions of interest were drawn inside and outside of the tissue at one plane and average intensity was measured. OD was calculated with the formula:  $\text{OD} = \log(\text{transmittance})/\text{thickness}$ . For transmission analysis, the mean intensity of the T-PMT channel was measured within a circular region of interest inside the tissue at 210  $\mu\text{m}$  from the edge and outside the tissue.

### Morphological changes

To assess morphological changes in cleared tissue, samples were imaged using a Leica MZ 12.5 stereo microscope. Tiles were stitched with the PhotoMerge function of Adobe Photoshop CC 2019 and perimeter measurements calculated with Image J.

### Detection of fluorescent signals in liver sections

Liver lobes were collected after sham or BDL laparotomy, fixed in 4% paraformaldehyde for 1 h, dehydrated in 30% sucrose/PBS at 4°C overnight and stored in Tissue-Tek OCT compound. Tissue was frozen at -80°C and sectioned by cryotome. Nuclei were counterstained with DAPI. Samples were then imaged with a Leica DM5500B IF microscope using Leica Suite Advanced Fluorescence 6000 software (Leica Microsystems, Wetzlar, Germany).

### Statistical analyses

Statistics were performed with GraphPad Prism Version 6.05 (GraphPad, CA, USA). Analysis of variance with post-hoc Tukey test was performed. A p-value of <0.05 was considered significant.

## Results & discussion

For this study, we sought to identify an OCA that effectively clears a lobe of liver while preserving GFP and tracer dye emissions. Based on prior published studies, we initially selected methods utilizing organic solvents (BABB and iDISCO) as well as three methods based on aqueous solvents (Sca/eS, SeeDB and UbasM) for our initial analyses. BABB's main reagents are benzyl alcohol and benzyl benzoate [35]. Its clearing performance is very good but its fluorescence profile (FP) and lipophilic dye compatibility are poor [28]. The iDISCO protocol sequentially utilizes tetrahydrofuran, dichloromethane and dibenzyl ether to clear tissue [37]. iDISCO produces good tissue clearing and is useful for immunofluorescence imaging; however, the reagents are highly noxious and require very careful handling [37]. The main components of Sca/eS are urea and sorbitol [23]. Its clearing ability is considered good, as are its FP and lipophilic dye capability [28]. SeeDB's primary reagent is fructose [24]. It has been shown to have moderate clearing capability and good FP and Di-I compatibility [28].

In preliminary experiments with UbasM, we observed substantial clearing of the liver within 24 h with only the initial incubation with Ub-1 reagent. We therefore included a modified 'Ub-1 protocol' in our comparative analysis (Figure 1). Among the protocols tested, UbasM required the longest processing time (7 days) but was methodologically simple, involving sequential incubations in three different solutions. The BABB, Sca/eS and SeeDB protocols required 3 days of processing but involved more steps. BABB involved progressive dehydrating/solvent incubations requiring multiple (but simple) solution changes, with reagents handled safely in a fume hood due to toxicity. The Sca/eS and SeeDB protocols involved relatively long incubation periods. In contrast, iDISCO was relatively expeditious in

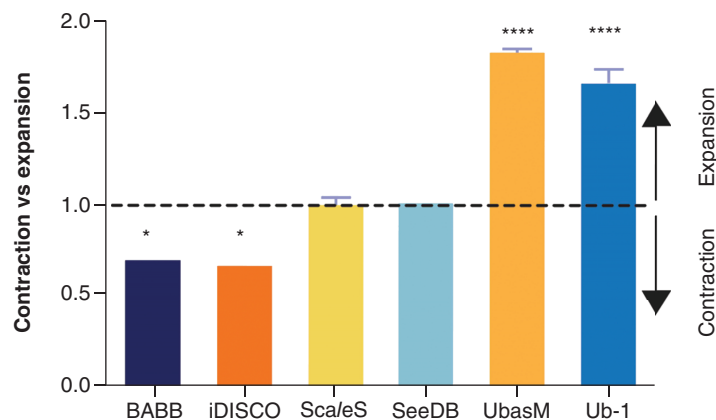


**Figure 2. Morphological changes.** Contraction and expansion of samples was evaluated to assess morphological changes. Surface area measurements were taken before and after clearing. Incubation of liver lobes in Ub-1 for 24 h resulted in less expansion than with UbasM ( $p = 0.021$ ). Error bars represent the standard deviation of measurement from nine replicates. Samples significantly different from one (no contraction or expansion) are shown with an asterisk. \* $p < 0.05$ ; \*\*\*\* $p < 0.0001$ .

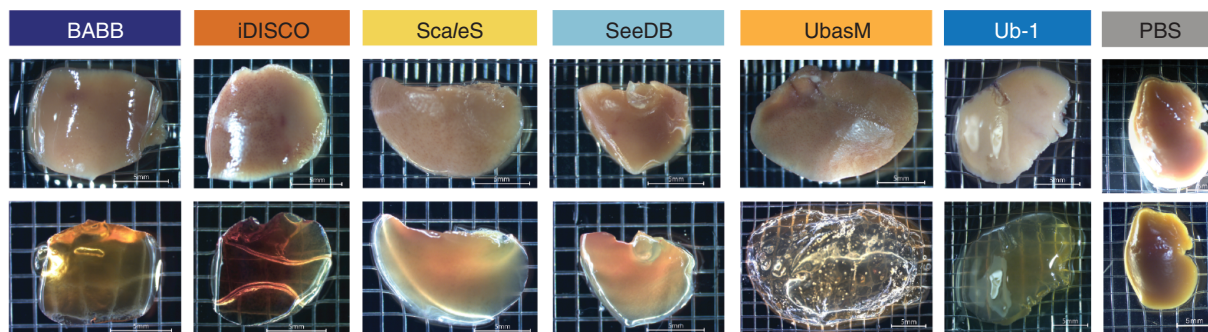


**Figure 3. Gross transparency comparison between methods.** Clearing performance was assessed with brightfield images before (top) and after clearing (bottom). Macroscopic transparency can be evaluated by visualizing the grid beneath samples. Crosshatch grid is  $2 \times 2$  mm.

terms of processing time (~27 h) but required careful handling of a toxicity class II solvent. Of the six methods we tested, the simplest was Ub-1, requiring just one solution with few components.

We assessed relative tissue expansion/contraction of our liver specimen with each OCA (Figure 2). Tissue distortion after clearing could potentially deform ultramicroscopic structures or disturb existing labels due to contraction, expansion or alterations of membrane or protein integrity [1,14,19,39]. These changes occur due to hyperhydrating, dehydrating or lipid-dissolving methods of action, though specific aqueous reagents have been formulated to optimize tissue stability with reproducible structural anatomy and fluorescent signals [23,24,28]. The literature, however, lacks a robust quantitative comparison of microstructural integrity preservation across reagents. Our results show that BABB and iDISCO shrunk samples due to dehydration and rendered tissues brittle. Sca/eS and SeeDB maintained tissue consistency with little expansion or contraction. UbasM expanded sample volumes to a significant degree (~180%) and tissues became gelatinous and tended to fall apart. The second reagent in the UbasM protocol, Ub-2, is meant to restore tissue to original volumes with a closer tissue RI match [28]. However, in our experiments, we found Ub-1 used alone for 24 h resulted in less expansion than with UbasM ( $p = 0.021$ ), with less observed tissue fragility.

To evaluate clearing efficacy, liver tissue transparency was assessed qualitatively via transmitted light microscopy (Figure 3). Both iDISCO and BABB rendered tissue very clear; however, both are known to quench endogenous fluorophore reporters because they are organic solvents [1,11,19,39]. Although Sca/eS and SeeDB have been demonstrated to preserve fluorescence and tissue structure very

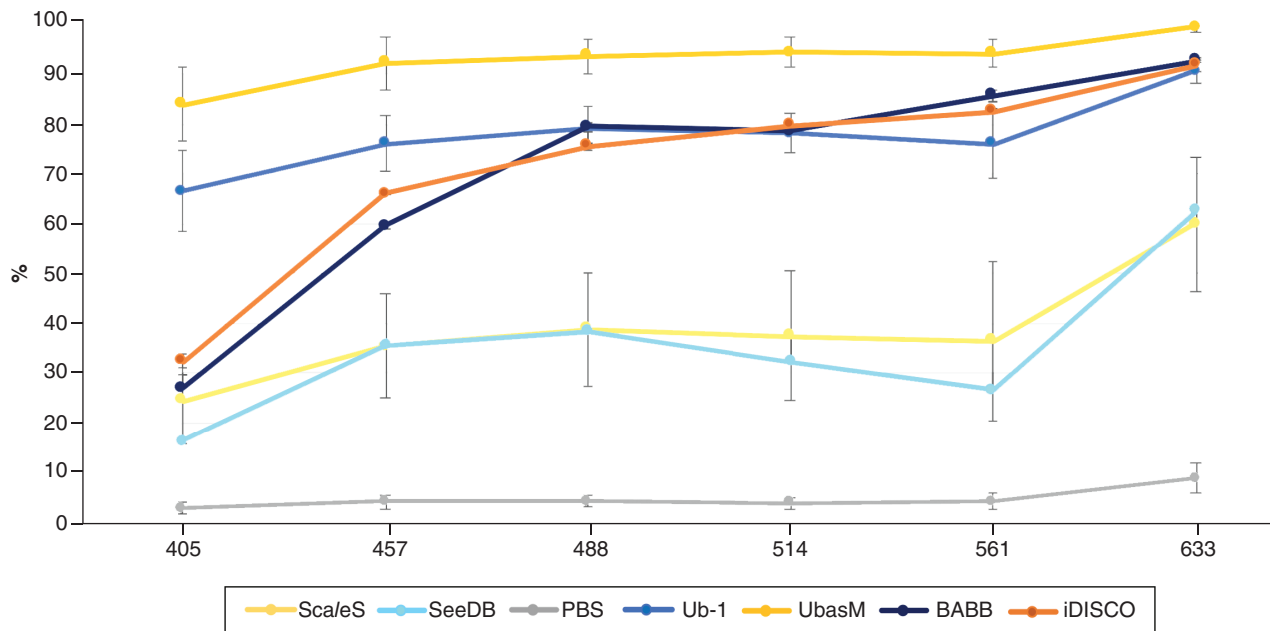


**Figure 4. Transmission analysis.** Transmission was compared in cleared samples at wavelengths 405, 457, 488, 514, 561 and 563 nm. Mean intensity of the T-PMT channel was measured within a circular region of interest inside the tissue at 210  $\mu\text{m}$  from the edge and just outside the tissue. Error bars represent the standard deviation of measurement from three or two replicates for iDISCO.

well [23,24], they cleared less effectively. UbasM and Ub-1 exhibited effective clearing in our comparison; additionally, being aqueous reagents, they were likely to preserve fluorescent protein signaling.

Next, we analyzed the fraction of light transmission of the cleared tissues at different wavelengths (Figure 4) and observed that UbasM had the highest transmission of all agents tested. The transmission of Ub-1-cleared tissue paralleled that of UbasM but was slightly lower across all wavelengths tested. Although Ub-1's transmission was slightly less than with UbasM, the Ub-1 procedure saves time in processing (1 week vs 1 day). For the three protocols that had the highest measured intensity, we performed OD.

We carried out OD analyses for BABB, UbasM and Ub-1, each of which performed well in terms of light transmission (Figure 5). The protocol that rendered the clearest (least optically dense) tissue across all wavelengths was UbasM; Ub-1 achieved a similar OD profile to UbasM in a much shorter time. BABB-cleared tissue was less clear at the blue end of the visible spectrum (405, 458 and 488 nm) but was similar to UbasM and Ub-1 at longer wavelengths (561 and 633 nm). Considering the popularity of BABB as an effective OCA, and that it has been particularly recommended for use in liver [29,30], these results were very promising for UbasM and Ub-1.

To assess preservation of protein and organic dye fluorescence by our modified Ub-1 clearing technique, we utilized *Prom1<sup>CreERT2-nLacZ/+</sup>;Rosa26<sup>Lsl-GFP</sup>* mice injected with tamoxifen to permanently label *Prom1*-expressing hepatic progenitor cells (HPCs) and their progeny with GFP. One week later, we injected lipophilic tracers (Di-I and Di-D) into the gallbladder and portal vein in order to label the intrahepatic bile ducts and the sinusoidal endothelium, respectively. We then collected the liver lobes, performed Ub-1 clearing and imaged the cleared tissue with confocal microscopy. Using high-resolution 3D rendering of confocal z-stack images, we were able to visualize the GFP<sup>+</sup> labeling, likely only in quiescent *Prom1*-expressing HPCs under basal noninjury conditions, either adjacent to or overlaid with Di-D-labeled endothelium of intrahepatic bile ducts (Figure 6 & Supplementary Video 1: [https://figshare.com/articles/media/Ub-1\\_optical\\_clearing\\_with\\_DiD\\_DiI\\_and\\_GFP\\_preservation\\_in\\_the\\_murine\\_liver\\_/12219950](https://figshare.com/articles/media/Ub-1_optical_clearing_with_DiD_DiI_and_GFP_preservation_in_the_murine_liver_/12219950)). We also observed uptake of Di-I in the pericentral but not periportal sinusoidal endothelium. Our observations were consistent with prior findings of the proximity of *Prom1*-expressing HPCs to biliary ductular cells [32,40]. The positive uptake of lipophilic dyes depicting intact branching ductular and vascular structures also emphasized that Ub-1 preserves membrane integrity. Our findings ultimately demonstrate the preservation of fluorescent labeling, including GFP and lipophilic dyes, following clearing by Ub-1.

To further assess Ub-1's applicability, we performed lineage tracing of fluorescently labeled cells using both traditional 2D tissue section histology and 3D microscopy after clearing to assess tissue structure and fluorescent labeling in a cholestatic injury model. Liver sections from *Prom1<sup>CreERT2-nLacZ/+</sup>;Rosa26<sup>mTmG</sup>* mice that underwent BDL or the sham operation were fluorescently stained and imaged by widefield microscopy. For comparison, *Prom1<sup>CreERT2-nLacZ/+</sup>;Rosa26<sup>Lsl-tdTomato</sup>;Col1a1<sup>GFP</sup>* mice also underwent BDL or the sham operation. At 2 weeks, Di-D was injected into the intrahepatic biliary tree to visualize the biliary system; liver lobes were then cleared and imaged by confocal microscopy. In 2D tissue sections, BDL livers compared with sham demonstrated increased expansion of GFP<sup>+</sup> *Prom1* HPC lineage within periportal regions (Figure 7A & B) [32,40]. Using Ub-1 to obtain greater 3D resolution, cleared livers demonstrated marked expansion of tdTomato<sup>+</sup> *Prom1*-expressing cells adjacent to as well as colocalized with the Di-D<sup>+</sup> biliary tree (Figure 8A

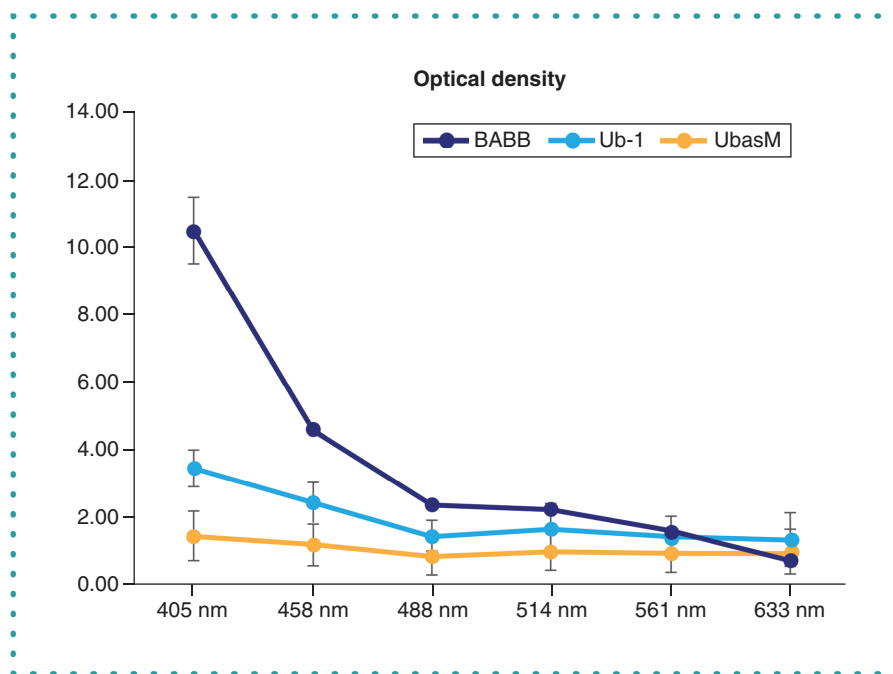


**Figure 5. Optical density.** Optical density of whole liver lobes was quantified to evaluate tissue transparency and clearing efficacy. Error bars represent the standard deviation of measurement from three replicates.

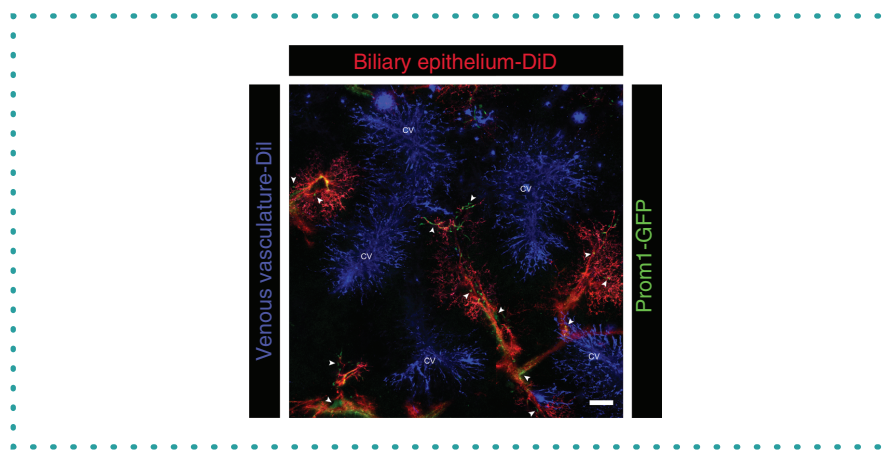


**Figure 6. Di-D, Di-I and green fluorescent protein preservation in the normal liver from tamoxifen-induced *Prom1<sup>CreERT2-nLacZ/+</sup>;Rosa26<sup>LsI-GFP</sup>* cleared with Ub-1.** Di-D labels biliary epithelium (red), Di-I labels venous vasculature (blue) and *Prom-1*-expressing hepatic progenitor cells (indicated by arrowheads) are labeled with GFP (green). CV indicates central vein. Images accompany 3D video rendered by confocal microscopy (Supplementary Video 1). Scale bar = 100  $\mu$ m.  
CV: Central vein; GFP: Green fluorescent protein.

& B & Supplementary Video 2A: [https://figshare.com/articles/media/Ub-1\\_optical\\_clearing\\_with\\_Col1a1GFP\\_tdTomato\\_and\\_DiD\\_preservation\\_in\\_sham\\_condition\\_in\\_the\\_murine\\_liver\\_/12219953](https://figshare.com/articles/media/Ub-1_optical_clearing_with_Col1a1GFP_tdTomato_and_DiD_preservation_in_sham_condition_in_the_murine_liver_/12219953) & Supplemental Video 2B: [https://figshare.com/articles/media/Ub-1\\_optical\\_clearing\\_with\\_Col1a1GFP\\_tdTomato\\_and\\_DiD\\_preservation\\_in\\_bile\\_duct\\_ligation\\_condition\\_in\\_the\\_murine\\_liver\\_/12219959](https://figshare.com/articles/media/Ub-1_optical_clearing_with_Col1a1GFP_tdTomato_and_DiD_preservation_in_bile_duct_ligation_condition_in_the_murine_liver_/12219959)). There was no observed colocalization of tdTomato with the expanded population of GFP<sup>+</sup> *Col1a1*-expressing myofibroblasts. Ub-1 combined with 3D microscopy therefore enabled successful appreciation of the volume of *Prom1* HPC progeny expansion, and their spatial proximity to myofibroblasts and intrahepatic biliary tree, in a comprehensive 3D perspective.

We conclude that our protocol using Ub-1 is favorable for use in optically clearing the murine liver, achieving adequate light transmission with adequate tissue preservation for the purpose of visualizing transgenically expressed reporter fluorophores and exogenously introduced lipophilic dyes. This protocol offers the advantage of simplicity in terms of solution preparation and minimal exchanges of incubation solutions. Moreover, our Ub-1 protocol accomplishes this in only 24 h. Further efforts are needed to determine whether

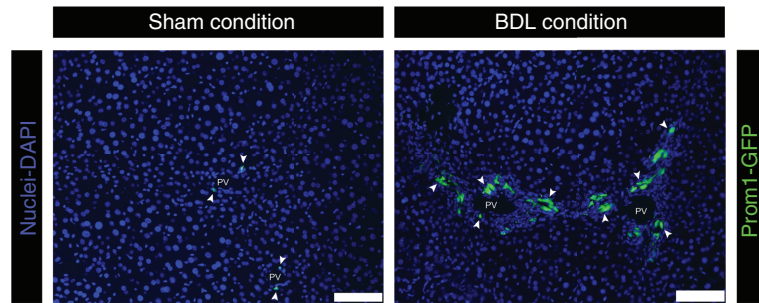


**Figure 7.** Detection of fluorescence emissions in liver sections from tamoxifen-induced *Prom1*<sup>Cre-ERT2-nLacZ/+</sup>; *Rosa26*<sup>mTmG</sup> mice that underwent bile duct ligation or sham operation. Murine liver sections prepared from (A) sham and (B) bile duct ligation were used for detection of GFP<sup>+</sup> *Prom1*-expressing hepatic progenitor cells (green, indicated by arrowheads). All cells that are not GFP<sup>+</sup> are tdTomato<sup>+</sup> (red). Nuclei were counterstained with DAPI (blue). Scale bar = 100  $\mu$ m. GFP: Green fluorescent protein; PV: Portal vein.

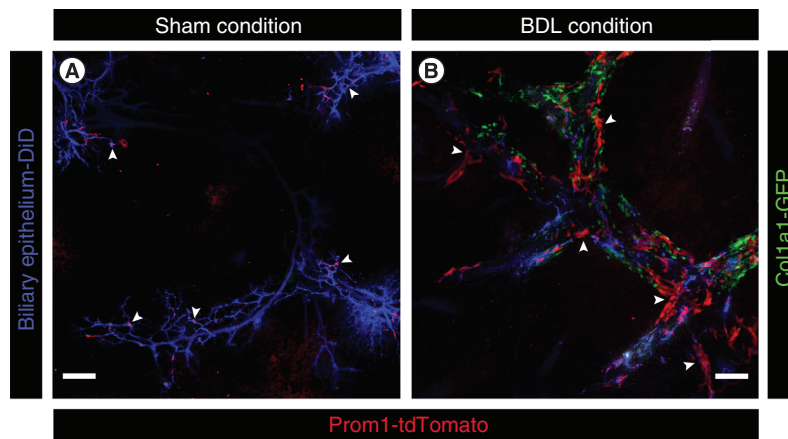


**Figure 8.** Ub-1 preserves emission of *Col1a1*-green fluorescent protein, tdTomato and Di-D tracer dye in sham and bile duct ligation condition in the livers of tamoxifen-induced *Prom1*<sup>CreERT2-nLacZ</sup>; *Rosa26*<sup>Lsl-tdTomato</sup>; *Col1a1*<sup>GFP</sup> mice. (A) Di-D-labeled bile ducts (blue) with sparse tdTomato-labeled *Prom-1*-expressing HPCs (red, indicated by arrowheads) and GFP-labeled *Col1a1*-expressing cells (green) proximally in the sham condition. (B) Di-D-labeled biliary tree (blue) shown with proliferative tdTomato-labeled *Prom-1*-expressing cells (red, indicated by arrowheads) and GFP-labeled *Col1a1*-expressing cells (green) in the bile duct ligation condition. Images accompany 3D video rendered by confocal microscopy (Supplementary Video 2A & B). Scale bar = 100  $\mu$ m. GFP: Green fluorescent protein; HPC: Hepatic progenitor cell.

immunofluorescence labeling of antigens is possible, as is the case with iDISCO. Our technique provides an adjunct to visualizing cell lineage tracing in the liver in three dimensions.

## Future perspective

An explosion of advances in optical tissue clearing and maturation of 3D imaging technologies has occurred in recent years. Simultaneously, the computing power necessary to visualize large 3D volumes at high resolution has become accessible to mainstream users. The nexus of modern clearing, imaging and computing technologies has given researchers unprecedented, complete views of whole tissues, organs and entire organisms, leading to insights that may be impossible to gain from traditional 2D imaging approaches such as tissue sectioning [14–16,41]. Imaging technologies, data processing and quantitative analysis capabilities will continue to improve, offering better visualization and quantification of data for users to draw insights from [42–44]. For example, OCAs have already enabled the discovery of a previously unknown subpleural acinar pattern in the lungs that has implications in recoil and tethering forces relevant in disease [45]. Efforts will evolve toward ultimately mapping human tissues to single-cell resolution. Emerging tools and techniques hold promise for observing developing processes at the molecular and cellular function level, and potentially guiding treatment models. Liu *et al.* [46] used OCAs with optical coherence tomography angiography to characterize port wine stain in human skin, facilitating treatment

decisions. Cremer *et al.* [47] used whole-mount clearing and fluorescent coronary angiography to discover diminished inflammation in a recurrent myocardial infarction mouse model, with the potential implication that post-infarction anti-inflammatory medications may have diminished utility as therapeutic interventions.

We present our approach for liver tissue clearing with the aim of accelerating discoveries that depend on knowledge about the 3D organization of not only the liver, but a variety of other organs. Because Ub-1 successfully clears liver tissue – a challenging organ to clear [12,16,28] – with excellent FP, we believe it can be used to clear other tissues for 3D imaging. Our protocol is likely compatible with immunofluorescence labeling, but for the purposes of this report, we did not successfully accomplish this. Future progress will likely lie in data/image capture technology which may enable less well-cleared tissues to still provide fluorescence information for digitized imaging purposes.

## Supplementary data

To view the supplementary data that accompany this paper please visit the journal website at: [www.future-science.com/doi/suppl/10.2144/btn-2020-0063](http://www.future-science.com/doi/suppl/10.2144/btn-2020-0063)

## Author contributions

M Hough and M Fenlon conceived the study. M Hough, A Glazier, C Short, M Fenlon, G Fernandez, E Mahdi and J Xu carried out the experiments. M Hough, A Glazier and C Short wrote the manuscript. C Short, E Mahdi, J Xu, G Fernandez, K Asahina and K Wang edited the manuscript.

## Financial & competing interests disclosure

This work was supported by NIH grants U01 DK084538 and R21 AA024840. The authors have no other relevant affiliations or financial involvement with any organization or entity with a financial interest in or financial conflict with the subject matter or materials discussed in the manuscript apart from those disclosed.

No writing assistance was utilized in the production of this manuscript.

## Ethical conduct of research

Mice used in this study were under a protocol approved by the Institutional Animal Care and Use Committee of the Saban Research Institute, Children's Hospital, Los Angeles, CA, USA.

## Open access

This work is licensed under the Attribution-NonCommercial-NoDerivatives 4.0 Unported License. To view a copy of this license, visit <http://creativecommons.org/licenses/by-nc-nd/4.0/>

## References

- Seo J, Choe M, Kim SY. Clearing and labeling techniques for large-scale biological tissues. *Mol. Cells* 39(6), 439–446 (2016).
- Costantini I, Cicchi R, Silvestri L, Vanzi F, Pavone FS. *In-vivo* and *ex-vivo* optical clearing methods for biological tissues: review. *Biomed. Opt. Express* 10(10), 5251–5267 (2019).
- Muntifering M, Castranova D, Gibson GA, Meyer E, Kofron M, Watson AM. Clearing for deep tissue imaging. *Curr. Protoc. Cytom.* 86(1), e38 (2018).
- Hong SM, Noë M, Hruban CA, Thompson ED, Wood LD, Hruban RH. A 'clearer' view of pancreatic pathology: a review of tissue clearing and advanced microscopy techniques. *Adv. Anat. Pathol.* 26(1), 31–39 (2019).
- Lloyd-Lewis B, Davis FM, Harris OB *et al.* Imaging the mammary gland and mammary tumours in 3D: optical tissue clearing and immunofluorescence methods. *Breast Cancer Res.* 18(1), 127 (2016).
- Lee E, Kim HJ, Sun W. See-through technology for biological tissue: 3-dimensional visualization of macromolecules. *Int. Neurobiol. J.* 20(Suppl. 1), S15–S22 (2016).
- Tainaka K, Kuno A, Kubota SI, Murakami T, Ueda HR. Chemical principles in tissue clearing and staining protocols for whole-body cell profiling. *Annu. Rev. Cell Dev. Biol.* 32, 713–741 (2016).
- Sdobnov AY, Darvin ME, Genina EA, Bashkatov AN, Lademann J, Tuchin VV. Recent progress in tissue optical clearing for spectroscopic application. *Spectrochim. Acta A Mol. Biomol. Spectrosc.* 197, 216–229 (2018).
- Zhu D, Larin KV, Luo Q, Tuchin VV. Recent progress in tissue optical clearing. *Laser Photon. Rev.* 7(5), 732–757 (2013).
- Wen X, Tuchin VV, Luo Q, Zhu D. Controlling the scattering of intralipid by using optical clearing agents. *Phys. Med. Biol.* 54(22), 6917–6930 (2009).
- Azaripour A, Lagerweij T, Scharfbillig C, Jadczyk AE, Willershausen B, Van Noorden CJ. A survey of clearing techniques for 3D imaging of tissues with special reference to connective tissue. *Prog. Histochem. Cytochem.* 51(2), 9–23 (2016).
- Xu J, Ma Y, Yu T, Zhu D. Quantitative assessment of optical clearing methods in various intact mouse organs. *J. Biophotonics* 12(2), e201800134 (2019).
- Wan P, Zhu J, Xu J, Li Y, Yu T, Zhu D. Evaluation of seven optical clearing methods in mouse brain. *Neurophotonics* 5(3), 035007 (2018).
- Susaki EA, Ueda HR. Whole-body and whole-organ clearing and imaging techniques with single-cell resolution: toward organism-level systems biology in mammals. *Cell Chem. Biol.* 23(1), 137–157 (2016).
- Husna N, Gascoigne NRJ, Tey HL, Ng LG, Tan Y. Reprint of 'Multi-modal image cytometry approach – from dynamic to whole organ imaging'. *Cell. Immunol.* 350, 104086 (2020).
- Sindhvani S, Syed AM, Wilhelm S, Chan WC. Exploring passive clearing for 3D optical imaging of nanoparticles in intact tissues. *Bioconjug. Chem.* 28(1), 253–259 (2017).
- Jing D, Zhang S, Luo W *et al.* Tissue clearing of both hard and soft tissue organs with the PEGASOS method. *Cell Res.* 28(8), 803–818 (2018).
- Tainaka K, Kubota SI, Suyama TQ *et al.* Whole-body imaging with single-cell resolution by tissue decolorization. *Cell* 159(4), 911–924 (2014).
- Lai HM, Ng WL, Gentleman SM, Wu W. Chemical probes for visualizing intact animal and human brain tissue. *Cell Chem. Biol.* 24(6), 659–672 (2017).
- Li Y, Xu J, Wan P, Yu T, Zhu D. Optimization of GFP fluorescence preservation by a modified uDISCO clearing protocol. *Front. Neuroanat.* 12, 67 (2018).
- Becker K, Jährling N, Saghaei S, Weiler R, Dodt HU. Chemical clearing and dehydration of GFP expressing mouse brains. *PLoS ONE* 7(3), e33916 (2012).
- Jensen KH, Berg RW. CLARITY-compatible lipophilic dyes for electrode marking and neuronal tracing. *Sci. Rep.* 6, 32674 (2016).
- Hama H, Hioki H, Namiki K *et al.* ScaleS: an optical clearing palette for biological imaging. *Nat. Neurosci.* 18(10), 1518–1529 (2015).

24. Ke MT, Fujimoto S, Imai T. SeeDB: a simple and morphology-preserving optical clearing agent for neuronal circuit reconstruction. *Nat. Neurosci.* 16(8), 1154–1161 (2013).
25. Yu T, Zhu J, Li Y *et al.* RTF: a rapid and versatile tissue optical clearing method. *Sci. Rep.* 8(1), 1964 (2018).
26. Hou B, Zhang D, Zhao S *et al.* Scalable and DiI-compatible optical clearance of the mammalian brain. *Front. Neuroanat.* 9, 19 (2015).
27. Kim JH, Jang MJ, Choi J *et al.* Optimizing tissue-clearing conditions based on analysis of the critical factors affecting tissue-clearing procedures. *Sci. Rep.* 8(1), 12815 (2018).
28. Chen L, Li G, Li Y *et al.* UbasM: an effective balanced optical clearing method for intact biomedical imaging. *Sci. Rep.* 7(1), 12218 (2017).
29. Kaneko K. Analysis for remodeling of hepatic tissue structures in 3D during regeneration. *Methods Mol. Biol.* 1905, 187–198 (2019).
30. Kamimoto K, Kaneko K, Kok CY, Okada H, Miyajima A, Itoh T. Heterogeneity and stochastic growth regulation of biliary epithelial cells dictate dynamic epithelial tissue remodeling. *Elife* 5, e15034 (2016).
31. Lee E, Choi J, Jo Y *et al.* ACT-PRESTO: rapid and consistent tissue clearing and labeling method for 3-dimensional (3D) imaging. *Sci. Rep.* 6, 18631 (2016).
32. Nguyen MV, Zagory JA, Dietz WH *et al.* Hepatic Prominin-1 expression is associated with biliary fibrosis. *Surgery* 161(5), 1266–1272 (2017).
33. Lua I, Li Y, Zagory JA *et al.* Characterization of hepatic stellate cells, portal fibroblasts, and mesothelial cells in normal and fibrotic livers. *J. Hepatol.* 64(5), 1137–1146 (2016).
34. Yata Y, Scanga A, Gillan A *et al.* DNase I-hypersensitive sites enhance alpha1(I) collagen gene expression in hepatic stellate cells. *Hepatology* 37(2), 267–276 (2003).
35. Kaneko K, Kamimoto K, Miyajima A, Itoh T. Adaptive remodeling of the biliary architecture underlies liver homeostasis. *Hepatology* 61(6), 2056–2066 (2015).
36. Dodt HU, Leischner U, Schierloh A *et al.* Ultramicroscopy: three-dimensional visualization of neuronal networks in the whole mouse brain. *Nat. Methods* 4(4), 331–336 (2007).
37. Renier N, Wu Z, Simon DJ, Yang J, Ariel P, Tessier-Lavigne M. iDISCO: a simple, rapid method to immunolabel large tissue samples for volume imaging. *Cell* 159(4), 896–910 (2014).
38. Schindelin J, Arganda-Carreras I, Frise E *et al.* Fiji: an open-source platform for biological-image analysis. *Nat. Methods* 9(7), 676–682 (2012).
39. Richardson DS, Lichtman JW. Clarifying tissue clearing. *Cell* 162(2), 246–257 (2015).
40. Mavila N, James D, Shivakumar P *et al.* Expansion of prominin-1-expressing cells in association with fibrosis of biliary atresia. *Hepatology* 60(3), 941–953 (2014).
41. Zhu L, Finkelstein D, Gao C *et al.* Multi-organ mapping of cancer risk. *Cell* 166(5), 1132–1146.e1137 (2016).
42. Pan C, Schoppe O, Parra-Damas A *et al.* Deep learning reveals cancer metastasis and therapeutic antibody targeting in the entire body. *Cell* 179(7), 1661–1676.e1619 (2019).
43. Nie J, Liu S, Yu T *et al.* Fast, 3D isotropic imaging of whole mouse brain using multiangle-resolved subvoxel SPIM. *Adv. Sci. (Weinh)* 7(3), 1901891 (2020).
44. Vinegoni C, Fumene Feruglio P, Courties G *et al.* Fluorescence microscopy tensor imaging representations for large-scale dataset analysis. *Sci. Rep.* 10(1), 5632 (2020).
45. Mitzner W, Loube J, Venezia J, Scott A. Self-organizing pattern of subpleural alveolar ducts. *Sci. Rep.* 10(1), 3185 (2020).
46. Liu Y, Zhu D, Xu J *et al.* Penetration-enhanced optical coherence tomography angiography with optical clearing agent for clinical evaluation of human skin. *Photodiagnosis Photodyn. Ther.* 30, 101734 (2020).
47. Cremer S, Schloss MJ, Vinegoni C *et al.* Diminished reactive hematopoiesis and cardiac inflammation in a mouse model of recurrent myocardial infarction. *J. Am. Coll. Cardiol.* 75(8), 901–915 (2020).